Preprints of the 21st IFAC World Congress (Virtual)
Berlin, Germany, July 12-17, 2020

Sequence Impedance-Based Stability Analysis of AC Microgrids Controlled by Virtual Synchronous Generator Control Methods ⋆

Marc Dokus, Frederik Stallmann and Axel Mertens *

* *Institute for Drive Systems and Power Electronics (IAL), Leibniz University Hannover, Hannover Germany, (e-mail: marc.dokus@ial.uni-hannover.de).*

Abstract: In this paper, sequence impedance-based modelling is applied to two different grid-forming converters which are based on virtual synchronous generator (VSG) concepts including a dual loop voltage control. The considered controls only differ in the feedback design (PLL-driven or not) of the power-related control loop. In general, impedance modelling is a suitable method to analyse stability issues related to converter controls for use in larger power networks. In this work, the analytical model of a voltage-controlled converter is illustrated first. Sequence impedance models are then proposed, which do not only predict the effect of two different VSG controls on the systems stability, but also reveal its frequency coupling effect and analogy to the classical droop control. In addition, a small power system consisting of VSG-controlled converters is analysed by their equivalent output impedances. These models and the stability of the converter cluster are validated by time-domain simulations and laboratory experiments. The close correlation between sequence impedance model, time-domain simulation and experimental results confirms the effectiveness of the derived models.

Keywords: Small-signal sequence impedance, harmonic stability, converter cluster, virtual synchronous generator, microgrid.

1. INTRODUCTION

In an effort to create a more sustainable power system, different concepts are deployed to interface solar and wind energy-based sources with electrical grids. Besides their differences, these power plants share some common characteristics. Due to their physical aspects (e.g. small power rating), the systems are called distributed energy resources (DER) which are mainly installed at the distribution grid level utilising a power electronic-based interface (Teodorescu et al., 2010). However, the high penetration of modern power systems by DER might increase their destabilising effects in the low (power-related control, e.g. droop or VSG control) to medium (inner current and voltage control) frequency range (Dokus and Mertens, 2019). These effects, which were first discovered in railway systems (Paice and Meyer, 2000), are often referred to as harmonic stability and have recently become more significant particularly for future grid scenarios (Farrokhabadi et al., 2019). Conventional stability definitions for large electrical grids (e.g. European grid) are missing these aspects (Kundur et al., 2004).

Different methods are proposed in the literature to address the issues of converter controller stability, namely: (a) Lyapunov functions (Shakerighadi et al., 2018; Kabalan et al., 2017); (b) phase portraits (Pan et al., 2019); (c) state space eigenvalues (Amin and Molinas, 2017); (d) impedance-based analysis (Wang et al., 2014). Among these techniques, (a) and (b) are directly applicable to non-linear systems which enables the analysis of power system stability in case of large signal transients. Unfortunately, these methods either require a model order reduction, in order to search for a Lyapunov function, or are restricted to low-order models. The techniques (c) and (d) are applicable to linear systems in time or frequency domain and require a linearisation of the power system equations while still keeping high-order models in the small-signal region. Especially, frequency domain modelling of converter systems as Norton/Thévenin equivalent is a promising approach to analyse controller stability issues in a non-linear system with a high number of states. In particular, the equivalent model can be reduced to the relevant subsystem that interacts with other grid components (here: impedance/admittance, cf. Section 3). Furthermore, linearising the system for a specific operation point provides the possibility to use standard small-signal stability analysis methods. In addition, the admittance/impedance of these converter systems can be shaped (passivated) by parameter tuning and additional controls using the analytical model to prevent these effects (Wang et al., 2017). When modelling a complete power system in this framework, detailed converter models can be applied to identify the contribution of each converter to the overall system behaviour (Wang et al., 2014). Thereby, the stability of large power systems regarding converter control issues

⋆ This work is supported by German Research Foundation DFG (project identification number 359921210).

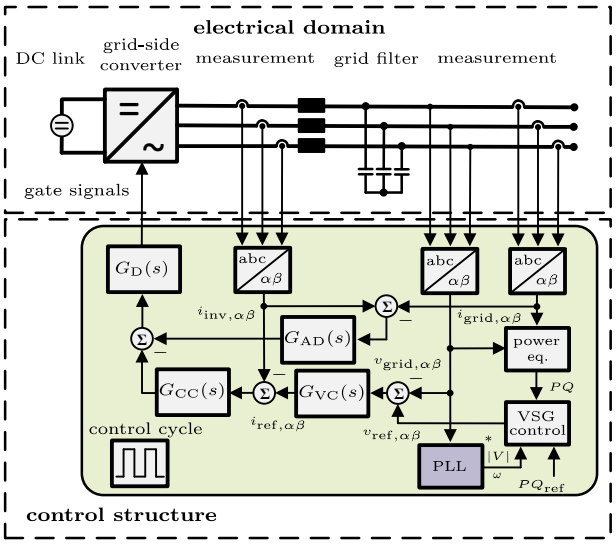

(a) Simplified structure of a grid-forming converter: inner control in the $\alpha\beta$-frame; power-related control based on internal $|V|$ and ω (VSG) or determined by PLL (vsgPLL*); transfer functions for active damping, current control, voltage control, PWM and sampling delay denoted as $G_{\mathrm{AD}}(s)$, $G_{\mathrm{CC}}(s)$, $G_{\mathrm{VC}}(s)$ and $G_{\mathrm{D}}(s)$, respectively

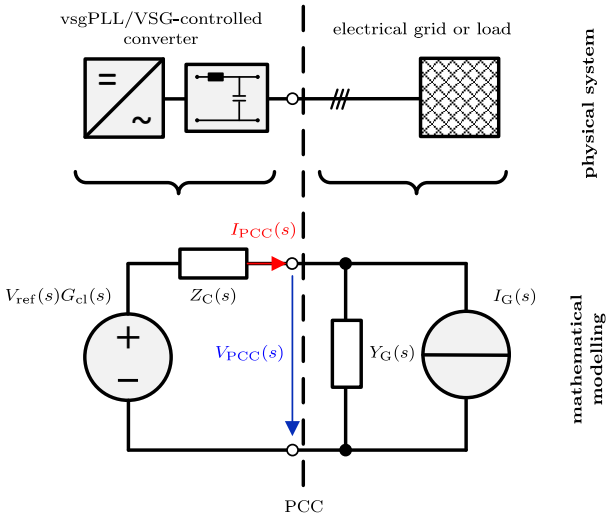

(b) Thévenin equivalent representation of a VSG and vsgPLL-controlled converter coupled with a Norton equivalent represenation of the electrical microgrid

Fig. 1. System under consideration: VSG and vsgPLL-controlled converter with a cascaded control structure coupled with an AC microgrid

can be systematically analysed. An exemplary case study for a conventional multi-level power system with several hundreds of converter systems is illustrated in (Sarstedt et al., 2019).

A variety of different white-box models covering all relevant control schemes is necessary to analyse the interoperability of converter clusters in future grid scenarios. The literature already covers a large number of impedance models, i.e. current-controlled converter in the $\alpha\beta$- (Wang et al., 2014) and dq-frame (Harnefors et al., 2007), the influence of phase-locked loops (PLL) and power control (Harnefors et al., 2016), voltage-controlled converter in the $\alpha\beta$- (Wang et al., 2014) and dq-frame (Wang et al., 2018), droop control in the $\alpha\beta$-frame (Dokus and Mertens, 2019), standard VSG control in the dq-frame (Wang et al., 2018) and an extension to cover effects at higher frequencies (Harnefors et al., 2017). Aside from the control aspect, the published impedance models are derived in the dq- or $\alpha\beta$-frame. The mathematical relations between these models are described in (Wang et al., 2018). The influence of an overlaying VSG control on the converter impedance has only been described for the standard approach in the dq-frame. An equivalent impedance model of two different VSG methods in the $\alpha\beta$-frame is systematically derived and experimentally verified in this paper to contribute to the stability analysis of converter systems in terms of VSG-controlled approaches.

In accordance with the literature, the term microgrid refers to the concept of an autonomous grid which allows the system operator to integrate a high penetration of power electronic-based energy generation into the main grid (Olivares et al., 2014; Rocabert et al., 2012). This approach is typically based on a multi-master concept using VSG and/or droop control for the individual voltage-controlled converters (Chandorkar et al., 1993). It enables an equal sharing of loads within the microgrid and leads to island capabilities (Ahn et al., 2010). Usually, a cascaded structure with an inner current and voltage control and an outer droop/VSG control is implemented (Vasquez et al., 2013; Wu et al., 2016). In many cases, the small-signal stability of microgrids is analysed by eigenvalues in the dq-frame or based on impedance models (Rasheduzzaman et al., 2014; Wu et al., 2016). Large signal phenomena are analysed using phase portrait-based concepts and Lyapunov functions. Due to the high number of system states, only small grid configurations are typically analysed in literature by eigenvalues or phase portraits. In addition, stability analysis based on Lyapunov functions is often limited to single converter entities (Kabalan et al., 2017; Shakerighadi et al., 2018).

As a contribution to the controller stability analysis of converter-dominated power systems, the authors' aim is to illustrate the small-signal characteristic of two different VSG methods as sequence impedances and apply these models to analyse stability issues in autonomous grids. In particular, the impact of applying the measured grid voltage phasor in the feedback path of grid-forming converters by a PLL is elaborated and compared with the standard VSG concept. Thereby, the presented models will extend the sequence impedance-based stability analysis of VSG-controlled AC microgrids.

The remainder of this paper is organised as follows. The VSG-controlled converter including voltage and current control in the $\alpha\beta$-frame is described in Section 2. Furthermore, impedance-based models of the converter control and the filter by means of symmetrical components is derived and the resulting representation is presented in Section 3. In addition, the coupling of this model with the

power system model is described. Section 4 validates the derived models by time-domain simulations and an example of a small-signal stability analysis is presented in order to illustrate the applicability. In Section 5, experimental results utilising a power hardware-in-the-loop (P-HIL) test setup are presented. Finally, Section 6 concludes the paper.

2. SYSTEM DESCRIPTION

2.1 Power-related Control of VSG-controlled VSC

Fig. 1a shows the typical power electronic-based interface of DER, namely a three-phase (3ph) two-level voltage source converter (VSC). In this work, only the grid-side converter is considered and the DC link is simplified as an ideal voltage source which provides energy to or consumes energy from the AC grid. The converter is connected to the electrical grid via an LC filter. The cascaded control structure of an outer voltage ($G_{\mathrm{VC}}(s)$ in Fig. 1a) and an inner current control loop ($G_{\mathrm{CC}}(s)$ in Fig. 1a) maintains the grid voltage at the point of common coupling (PCC). The voltage reference is generated by the following VSG equations (VSG control in Fig. 1a) described in s-domain

$$\omega_{\mathrm{ref}} = \frac{1}{sJ_{\mathrm{p}}\omega_{\mathrm{N}}}\big(P_{\mathrm{ref}} - P + D_{\mathrm{p}}(\omega_{\mathrm{N}} - \omega)\big), \quad (3)$$

$$\hat{V}_{\mathrm{ref}} = \frac{1}{sJ_{\mathrm{q}}}\big(Q_{\mathrm{ref}} - Q + D_{\mathrm{q}}(\hat{V}_{\mathrm{N}} - \hat{V})\big), \quad (4)$$

with $\{\omega, \hat{V}\} = \{\omega_{\mathrm{ref}}, \hat{V}_{\mathrm{ref}}\}$ or estimated by a PLL,

where $D_{\mathrm{p}}/D_{\mathrm{q}}$ are the frequency and voltage droop coefficient; $J_{\mathrm{p}}/J_{\mathrm{q}}$ are the virtual inertia for frequency and voltage; $\omega_{\mathrm{N}}/\hat{V}_{\mathrm{N}}$ are the nominal frequency and voltage amplitude; $P_{\mathrm{ref}}/Q_{\mathrm{ref}}$ are the reference values for active and reactive power; P/Q are the measured active and reactive power. The voltage and frequency feedback in Fig. 1a and (3) - (4) are denoted as $\hat{V}/\omega$, determined in literature either by the reference values $\hat{V}_{\mathrm{ref}}/\omega_{\mathrm{ref}}$ (variation 1: VSG) or less often estimated by a PLL (variation 2: vsgPLL, violet* in Fig. 1a). The measured active and reactive power is calculated (power eq. in Fig. 1a) based on the unfiltered grid currents $i_{\mathrm{grid},\alpha\beta}$ and grid voltages $v_{\mathrm{grid},\alpha\beta}$ transformed to the $\alpha\beta$-frame

$$P = \frac{3}{2}\big(v_{\mathrm{grid},\alpha} i_{\mathrm{grid},\alpha} + v_{\mathrm{grid},\beta} i_{\mathrm{grid},\beta}\big), \quad (5)$$

$$Q = \frac{3}{2}\big(v_{\mathrm{grid},\beta} i_{\mathrm{grid},\alpha} - v_{\mathrm{grid},\alpha} i_{\mathrm{grid},\beta}\big). \quad (6)$$

2.2 Inner Control of VSG-controlled VSC

The inner converter control in Fig. 1a is implemented in the $\alpha\beta$-frame utilising discrete proportional + resonant controller $\big(G_{\mathrm{CC}}(s)$ and $G_{\mathrm{VC}}(s)\big)$ while the inherent PWM and sampling delay is described by $G_{\mathrm{D}}(s)$. Since controlling of harmonics can be essential to guarantee an appropriate power quality in microgrids, the fundamental frequency and harmonics up to the 13^{th} order are covered by the resonant controller. As a consequence, a phase lead and an active damping method ($G_{\mathrm{AD}}(s)$ in Fig. 1a) based on the capacitor current $i_{\mathrm{C},\alpha\beta} = i_{\mathrm{inv},\alpha\beta} - i_{\mathrm{grid},\alpha\beta}$ (Wang et al., 2015; Parker et al., 2014) are implemented. The voltage control is implemented as an outer control loop providing a reference for the current control. The design of this cascaded control structure is described in (Vasquez et al., 2013). The transfer functions of the control in Fig. 1a are expressed by the following equations

$$G_{\mathrm{CC}}(s)=k_{\mathrm{P,I}}\Bigg(1+\frac{1}{T_{1,\mathrm{I}}}\frac{2\omega_{\mathrm{BW,I}}(s\cos\phi_{1,\mathrm{I}}-\omega_0\sin\phi_{1,\mathrm{I}})}{s^2+2\omega_{\mathrm{BW,I}}s+\omega_0^2}\ldots + \sum_{h=5,7..}^{13}\frac{1}{T_{h,\mathrm{I}}}\frac{2\omega_{\mathrm{BW,I}}(s\cos\phi_{h,\mathrm{I}}-h\omega_0\sin\phi_{h,\mathrm{I}})}{s^2+2\omega_{\mathrm{BW,I}}s+h^2\omega_0^2}\Bigg), \quad (7)$$

$$G_{\mathrm{VC}}(s)=k_{\mathrm{P,V}}\Bigg(1+\frac{1}{T_{1,\mathrm{V}}}\frac{2\omega_{\mathrm{BW,V}}(s\cos\phi_{1,\mathrm{V}}-\omega_0\sin\phi_{1,\mathrm{V}})}{s^2+2\omega_{\mathrm{BW,V}}s+\omega_0^2}\ldots + \sum_{h=5,7..}^{13}\frac{1}{T_{h,\mathrm{V}}}\frac{2\omega_{\mathrm{BW,V}}(s\cos\phi_{h,\mathrm{V}}-h\omega_0\sin\phi_{h,\mathrm{V}})}{s^2+2\omega_{\mathrm{BW,V}}s+h^2\omega_0^2}\Bigg), \quad (8)$$

$$G_{\mathrm{AD}}(s) = \frac{K_{\mathrm{rc}}s}{s+\omega_{\mathrm{rc}}}, \quad (9)$$

$$G_{\mathrm{D}}(s) = \frac{e^{-sT_{\mathrm{s}}} - e^{-s2T_{\mathrm{s}}}}{sT_{\mathrm{s}}}, \quad (10)$$

where the controllers are defined by a proportional and integral gain k_{P}/T_h, a phase lead ϕ_h and a defined bandwidth ω_{BW} for the resonant part; T_{s} denotes the sampling period. The proportional gain K_{rc} and the bandwidth ω_{rc} are parameters of the active damping method.

2.3 Electrical Power System

An AC microgrid consisting of standard VSG- or vsgPLL-controlled converters is considered in this work. The electrical grid in Fig. 1b is represented by a Norton equivalent for the sake of simplicity when deriving the controller stability criterion in Section 3.4. In general, any combination of current- and voltage-controlled sources/loads can be covered by coupling their Norton and Thévenin equivalents.

3. SYSTEM MODELLING

3.1 Inner Current and Voltage Control

The equivalent representation of a vsgPLL and VSG-controlled converter as a voltage source with an impedance is illustrated in Fig. 1b and will be derived in the following section. The model is based on the Thévenin model of a voltage-controlled converter published in (Wang et al., 2014) and can be described by (1) and (2), where L and C denote the inductance and capacitance of the LC filter. The filter resistances are neglected to reduce the complexity of the transfer functions. Here, positive- and negative-sequence impedances are the same. Furthermore, $Z_{\mathrm{C}}(s)$ in Fig. 1b equals $Z_{\mathrm{VC}}(s)$, if only voltage control is considered.

$$G_{\mathrm{cl}}(s) = \frac{G_{\mathrm{CC}}(s)G_{\mathrm{VC}}(s)G_{\mathrm{D}}(s)}{CLs^2 + CG_{\mathrm{AD}}(s)G_{\mathrm{D}}(s)s + CG_{\mathrm{CC}}(s)G_{\mathrm{D}}(s)s + G_{\mathrm{CC}}(s)G_{\mathrm{VC}}(s)G_{\mathrm{D}}(s) + 1} \quad (1)$$

$$Z_{\mathrm{VC}}(s) = \frac{Ls + G_{\mathrm{CC}}(s)G_{\mathrm{D}}(s)}{CLs^2 + CG_{\mathrm{AD}}(s)G_{\mathrm{D}}(s)s + CG_{\mathrm{CC}}(s)G_{\mathrm{D}}(s)s + G_{\mathrm{CC}}(s)G_{\mathrm{VC}}(s)G_{\mathrm{D}}(s) + 1} \quad (2)$$

3.2 Phase-locked Loop

In case of the vsgPLL control method, $\{\omega, \hat{V}\}$ in (3) - (4) are determined by a stationary reference frame (SRF) PLL algorithm, which can be included in this description by linearising the system for a specific operation point defined by $\boldsymbol{v_{PCC}} = \hat{V}_0 e^{j\varphi_u}$ and $\omega = \omega_N$. Small-signal voltage perturbations $\boldsymbol{dV}(\widetilde{s})$ with the disturbance frequency $\widetilde{s} = j\omega_d$ and $\varphi_u = 0°$ are introduced in (11) to derive a small-signal PLL model

$$\boldsymbol{V_{PCC}}(\widetilde{s}) = \big(\hat{V}_0 + \boldsymbol{dV}(\widetilde{s})\big). \tag{11}$$

In practical cases, a DSOGI-based filter $G_{DS}(s)$ is often implemented to extract the fundamental frequency (Teodorescu et al., 2010). A simple PI-controller ($k_{P,PLL}$ and $T_{I,PLL}$) tracks the voltage phase by adjusting $\omega(\widetilde{s}) = \omega_N + \Delta\omega(\widetilde{s})$. Thus, a PLL can be described by

$$\begin{aligned}\Delta\omega(\widetilde{s}) &= \left(k_{P,PLL} + \frac{1}{\widetilde{s} T_{I,PLL}}\right) \mathrm{Im}\{G_{DS}(s)\boldsymbol{V_{PCC}}(\widetilde{\boldsymbol{s}}) e^{-j\boldsymbol{d\delta}(\widetilde{\boldsymbol{s}})}\} \\ &= G_{PLL,c}\mathrm{Im}\{G_{DS}(s)\boldsymbol{V_{PCC}}(\widetilde{\boldsymbol{s}}) e^{-j\boldsymbol{d\delta}(\widetilde{\boldsymbol{s}})}\}. \end{aligned} \tag{12}$$

Applying the same simplifications as in (Harnefors et al., 2007) yields the necessary small-signal transfer functions of the PLL

$$\boldsymbol{d\omega}(\widetilde{\boldsymbol{s}}) = G_{PLL}(\widetilde{s})\,\mathrm{Im}\{G_{DS}(s)\boldsymbol{dV}(\widetilde{s})\}, \tag{13}$$

$$\boldsymbol{d\hat{V}}(\widetilde{\boldsymbol{s}}) = \mathrm{Re}\{G_{DS}(s)\boldsymbol{dV}(\widetilde{s})\}. \tag{14}$$

The transfer function $G_{PLL}(\widetilde{s})$ describes the closed loop PLL tracking performance and is defined as

$$G_{PLL}(\widetilde{s}) = \frac{G_{PLL,c}(\widetilde{s})\widetilde{s}}{\hat{V}_0 G_{PLL,c}(\widetilde{s}) + \widetilde{s}}. \tag{15}$$

3.3 Linearised vsgPLL/VSG Control

A linearised model of the vsgPLL/VSG control can be derived for a specific operation point by applying (11) and describing the current at the point of common coupling as

$$\boldsymbol{I_{PCC}}(\widetilde{s}) = \big(\hat{i}_0 e^{j(\varphi_u - \varphi_i)} + \boldsymbol{di}(\widetilde{s})\big), \tag{17}$$

where $\boldsymbol{i_{PCC}} = \hat{i}_0 e^{j\varphi_i}$ is the steady-state current and $\boldsymbol{di}(\widetilde{s})$ is a small-signal current perturbation with the disturbance frequency $\widetilde{s} = j\omega_d$.

The small-signal impact of these perturbations on the vsgPLL/VSG control can be analysed by substituting the active and reactive power with

$$\boldsymbol{S}(\widetilde{s}) = P(\widetilde{s}) + jQ(\widetilde{s}) = \frac{3}{2}\boldsymbol{V_{PCC}}(\widetilde{s})\overline{\boldsymbol{I}}_{\boldsymbol{PCC}}(\widetilde{s}) \tag{18}$$

in (3) and (4). In particular, $\overline{\boldsymbol{I}}_{\boldsymbol{PCC}}(\widetilde{s})$ denotes the conjugate complex of $\boldsymbol{I_{PCC}}(\widetilde{s})$. Neglecting any cross coupling between $\boldsymbol{di}(\widetilde{s})$ and $\boldsymbol{dV}(\widetilde{s})$ yields the following vsgPLL and VSG equations:

$$\begin{aligned}\boldsymbol{d\theta_{ref}}(\widetilde{s}) = -\frac{1}{\omega_N J_p \widetilde{s}^2}\Bigg(&\frac{3}{2}\mathrm{Re}\{\hat{V}_0 \times \overline{\boldsymbol{di}}(\widetilde{s})\} + \frac{3}{2}\mathrm{Re}\{\boldsymbol{dV}(\widetilde{s}) \times \overline{\boldsymbol{i_0}}\} \ldots \\ &+ D_p \boldsymbol{d\omega}(\widetilde{s})\Bigg), \end{aligned} \tag{19}$$

$$\begin{aligned}\boldsymbol{d\hat{V}_{ref}}(\widetilde{s}) = -\frac{1}{J_q \widetilde{s}}\Bigg(&\frac{3}{2}\mathrm{Im}\{\hat{V}_0 \times \overline{\boldsymbol{di}}(\widetilde{s})\} + \frac{3}{2}\mathrm{Im}\{\boldsymbol{dV}(\widetilde{s}) \times \overline{\boldsymbol{i_0}}\} \ldots \\ &+ D_q \boldsymbol{d\hat{V}}(\widetilde{s})\Bigg), \end{aligned} \tag{20}$$

with $\{\boldsymbol{d\omega}, \boldsymbol{d\hat{V}}\} = \{\boldsymbol{d\omega_{ref}}, \boldsymbol{d\hat{V}_{ref}}\}$: VSG,
or $\{\boldsymbol{d\omega}, \boldsymbol{d\hat{V}}\} = \{(13), (14)\}$: vsgPLL,

where $\boldsymbol{i_0} = \hat{i}_0 e^{j(\varphi_u - \varphi_i)}$ is used for the sake of brevity. In case of a PLL-driven concept, neglecting cross coupling is valid as long as the PLL bandwidth is higher than the one of the VSG control.

Furthermore, the reference voltage phasor in Fig. 1a can be expressed as

$$\boldsymbol{V_{ref}}(s) = \big(\hat{V}_0 + \boldsymbol{d\hat{V}_{ref}}(\widetilde{s})\big) e^{j(\boldsymbol{d\theta_{ref}}(\widetilde{s}) + \omega_N t)} \tag{21}$$

in the $\alpha\beta$-frame. In addition, it should be noted that the resulting frequency $s = j\omega$ is the sum of the disturbance frequency $\widetilde{s} = j\omega_d$ and the frequency $j\omega = j\omega_N$ of the linearised operation point.

In case of a voltage-controlled converter, the PCC voltage can be described as

$$\boldsymbol{V_{PCC}}(s) = G_{cl}(s)\boldsymbol{V_{ref}}(s) - Z_{VC}(s)\boldsymbol{I_{PCC}}(s) \tag{22}$$

by substituting $Z_C(s) = Z_{VC}(s)$ in Fig. 1b.

The analytical model of a vsgPLL/VSG-controlled converter can be derived by simplifying (21), utilising the relation $e^{j(\boldsymbol{d\theta_{ref}}(s) + \omega_N t)} \approx \big(1 + j\boldsymbol{d\theta_{ref}}(s)\big) e^{j\omega_N t}$ and neglecting cross coupling between $\boldsymbol{d\theta_{ref}}(s)$ and $\boldsymbol{d\hat{V}_{ref}}(s)$ which yields

$$\boldsymbol{dV_{ref}}(s) = \Big(\boldsymbol{d\hat{V}_{ref}}(\widetilde{s}) + j\boldsymbol{d\theta_{ref}}(\widetilde{s})V_0\Big) e^{j\omega_N t}. \tag{23}$$

Finally, merging (23), (19) and (20) with (22) and applying the relation $\mathrm{Im}\{X\} = \frac{X - \overline{X}}{2j}$ and $\mathrm{Re}\{X\} = \frac{X + \overline{X}}{2}$ yield the equation system for the complete system

---

For positive-sequence perturbations, the following equation system is valid:

$$\mathbf{A} = \begin{bmatrix} 1 + \frac{3}{4}\overline{\boldsymbol{i_0}} G_{cl}(s) j \left(\frac{\hat{V}_0}{\omega_N D_p + \omega_N J_p (s - j\omega_N)(s - j\omega_N)} - \frac{1}{D_q + J_q(s - j\omega_N)}\right) + \frac{1}{2} G_{cl}(s) G_{DS}(s) \left(\frac{D_p \hat{V}_0 G_{PLL}(s - j\omega_N)}{J_p (s - j\omega_N)} \frac{1}{s - j\omega_N} + \frac{D_q}{J_q(s - j\omega_N)}\right) & \ldots \\ \frac{3}{4}\boldsymbol{i_0} G_{cl}(2j\omega_N - s) j \left(\frac{\hat{V}_0}{\omega_N D_p + \omega_N J_p (j\omega_N - s)(j\omega_N - s)} + \frac{1}{D_q + J_q(j\omega_N - s)}\right) - \frac{1}{2} G_{cl}(2j\omega_N - s) G_{DS}(2j\omega_N - s) \left(\frac{D_p \hat{V}_0 G_{PLL}(j\omega_N - s)}{J_p (j\omega_N - s)} \frac{1}{j\omega_N - s} - \frac{D_q}{J_q(j\omega_N - s)}\right) & \ldots \\ \frac{3}{4}\boldsymbol{i_0} G_{cl}(s) j \left(\frac{\hat{V}_0}{\omega_N D_p + \omega_N J_p (s - j\omega_N)(s - j\omega_N)} + \frac{1}{D_q + J_q(s - j\omega_N)}\right) - \frac{1}{2} G_{cl}(s) G_{DS}(s) \left(\frac{D_p \hat{V}_0 G_{PLL}(s - j\omega_N)}{J_p (s - j\omega_N)} \frac{1}{s - j\omega_N} - \frac{D_q}{J_q(s - j\omega_N)}\right) & \\ 1 + \frac{3}{4}\overline{\boldsymbol{i_0}} G_{cl}(2j\omega_N - s) j \left(\frac{\hat{V}_0}{\omega_N D_p + \omega_N J_p (j\omega_N - s)(j\omega_N - s)} - \frac{1}{D_q + J_q(j\omega_N - s)}\right) + \frac{1}{2} G_{cl}(2j\omega_N - s) G_{DS}(2j\omega_N - s) \left(\frac{D_p \hat{V}_0 G_{PLL}(j\omega_N - s)}{J_p (j\omega_N - s)} \frac{1}{j\omega_N - s} + \frac{D_q}{J_q(j\omega_N - s)}\right) & \end{bmatrix}$$

$$\underline{B} = \begin{bmatrix} -Z_{VC}(s) - j\frac{3}{4}\hat{V}_0 G_{cl}(s) \left(\hat{V}_0 \frac{1}{\omega_N D_p + \omega_N J_p (s - j\omega_N)(s - j\omega_N)} + \frac{1}{D_q + J_q(s - j\omega_N)}\right) \\ -j\frac{3}{4}\hat{V}_0 G_{cl}(2j\omega_N - s) \left(\hat{V}_0 \frac{1}{\omega_N D_p + \omega_N J_p (j\omega_N - s)(j\omega_N - s)} - \frac{1}{D_q + J_q(j\omega_N - s)}\right) \end{bmatrix} \boldsymbol{di}(s) \tag{16}$$

$$\underline{x} = \begin{bmatrix} \boldsymbol{dV}(s) \\ \boldsymbol{dV}(2j\omega_N - s) \end{bmatrix}$$

with highlighted terms in case of VSG or vsgPLL control

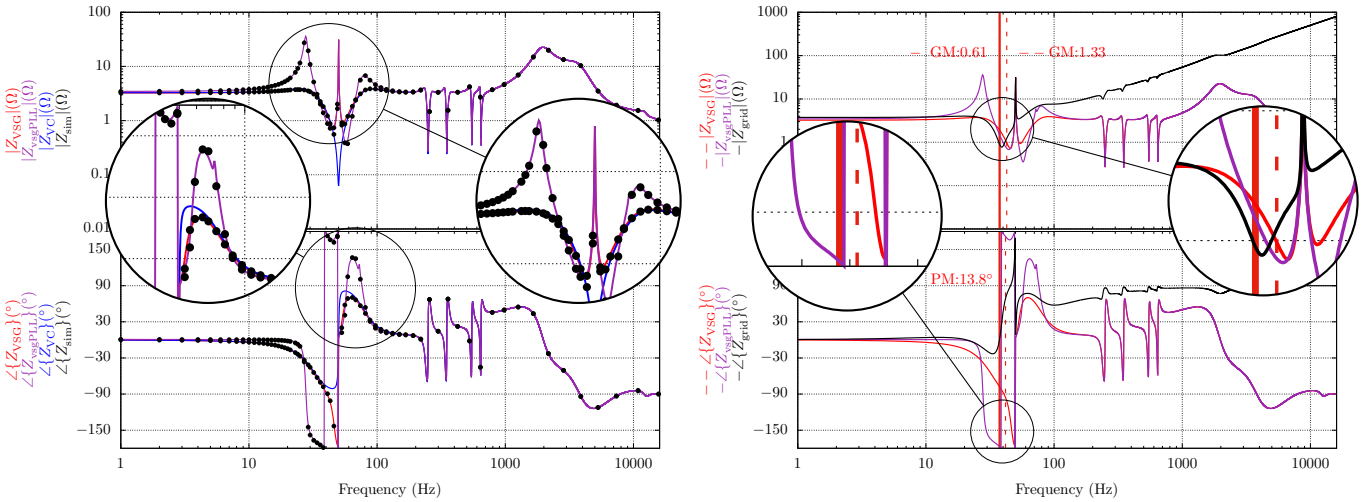

(a) Frequency sweep from 1 Hz to 16 kHz for positive-sequence impedance of voltage-controlled converter $Z_{\mathrm{VC}}(s)$, VSG-controlled converter $Z_{\mathrm{VSG}}(s)$, vsgPLL-controlled converter $Z_{\mathrm{vsgPLL}}(s)$ and time-domain simulation $Z_{\mathrm{sim}}(s)$

(b) Stability analysis of the application example: $\frac{Z_{\mathrm{C}}(s)}{Z_{\mathrm{grid}}(s)}$ needs to fulfil the Nyquist criterion; $Z_{\mathrm{grid}}(s)$: Impedance at PCC; $Z_{\mathrm{VSG}}(s)$ (dashed): Impedance of VSG-controlled converter; $Z_{\mathrm{vsgPLL}}(s)$ (solid): Impedance of vsgPLL-controlled converter

Fig. 2. Analysis and modelling of vsgPLL- and VSG-controlled converters, whose parameters are listed in Table 1

$$\mathbf{A}\begin{pmatrix}\square\square\\ \square\square\end{pmatrix}\underline{x}\begin{pmatrix}\square\\ \square\end{pmatrix}=\underline{B}\begin{pmatrix}\square\\ \square\end{pmatrix}, \tag{24}$$

which is described in detail in (16).

The final converter output impedance $Z_{\mathrm{C}}(s) = \frac{\boldsymbol{dV}(s)}{\boldsymbol{di}(s)}$ can be extracted by solving the linear system in (16). In this case, $Z_{\mathrm{C}}(s)$ differs for positive- and negative-sequence perturbations $\boldsymbol{di}(s)$. In literature, the additional component $\boldsymbol{dV}(2j\omega_{\mathrm{N}} - s)$ is often called an image or mirrored harmonic and can be included in the small-signal stability analysis by following the steps in (Vieto and Sun, 2018).

3.4 Coupling of Converter and Grid Models

The small-signal stability of power networks can be analysed in this framework by coupling the derived model with admittance/impedance models for all other grid-connected devices including loads (see Fig. 1b). Thus, the PCC voltage can further be described by the closed loop transfer function including the merged grid admittance $Y_{\mathrm{G}}(s)$ connected to the converter terminal as

$$V_{\mathrm{PCC}}(s) = \frac{G_{\mathrm{cl}}(s)V_{\mathrm{ref}}(s)}{1+Y_{\mathrm{G}}(s)Z_{\mathrm{C}}(s)} - \frac{Z_{\mathrm{C}}(s)I_{\mathrm{G}}(s)}{1+Y_{\mathrm{G}}(s)Z_{\mathrm{C}}(s)}. \tag{25}$$

From the perspective of control theory, $G_{\mathrm{cl}}(s)$ in Fig. 1b needs to be designed for an appropriate transient response while guaranteeing a reasonable phase and gain margin. In addition, stability is only guaranteed, if the minor feedback $Y_{\mathrm{G}}(s)Z_{\mathrm{C}}(s)$ fulfils the General Nyquist Criterion (GNC). This analysis has to be done for every controlled converter system and their point of common coupling.

4. SIMULATION RESULTS

4.1 Model Validation

The derived models are validated by time-domain simulations in MATLAB/Simulink combined with the PLECS toolbox. In order to extract the equivalent impedance at each frequency, switched Electromagnetic Transient (EMT) models of the converter systems in Fig. 1a are operated in steady state, while a small positive-sequence current perturbation is injected. All relevant parameters of these converters are listed in Table 1. The analytically derived and extracted impedances are illustrated in Fig. 2a as amplitude and phase.

The equivalent impedances of both small-signal models correspond to the detailed time-domain models. In addition, the influence of the VSG control is restricted to small frequencies around the operation point $\omega = \omega_{\mathrm{N}}$ analogously to a droop-controlled converter with $D_{\mathrm{p}} = -\frac{P_{\mathrm{N}}}{m_{\omega}\omega_{\mathrm{N}}}$, $D_{\mathrm{q}} = -\frac{P_{\mathrm{N}}}{m_{\mathrm{V}}}$, $J_{\mathrm{p}} = \frac{D_{\mathrm{p}}}{\omega_{\mathrm{LP}}}$ and $J_{\mathrm{q}} = \frac{D_{\mathrm{q}}}{\omega_{\mathrm{LP}}}$ in (Dokus and

Table 1. Simulation Parameters

PARAMETER	SYMBOL	VALUE
Rated Power	P_{N}	16 kW
Rated Voltage	V_{N}	400 V
Rated Frequency	f_{N}	50 Hz
Active Power Reference	P_{ref}	16 kW
Reactive Power Reference	Q_{ref}	0 kVar
Voltage @ steady state	$V_{0,\mathrm{RMS,LL}}$	400 V
Power @ steady state	PQ_0	PQ_{ref}
Nominal Frequency	ω_{N}	314.16 $\frac{\mathrm{rad}}{\mathrm{s}}$
Sampling Time	T_{s}	62.5 μs
Filter Inductor	L	900 μH
Filter Capacitor	C	10 μF
Frequency Droop Coefficient	D_{p}	16.21
Voltage Droop Coefficient	D_{q}	979.80
Virtual Frequency Inertia	J_{p}	0.129
Virtual Voltage Inertia	J_{q}	7.797
Nominal Frequency of DSOGI Filter	$\omega_{\mathrm{N,DSOGI}}$	314.16 $\frac{\mathrm{rad}}{\mathrm{s}}$
P. Gain - DSOGI Filter	k	$\sqrt{2}$
P. Gain - PLL	$k_{\mathrm{P,PLL}}$	1.633
I. Time Constant - PLL	$T_{\mathrm{i,PLL}}$	–
P. Gain - Current Control	$k_{\mathrm{P,I}}$	4.40
P. Gain - Voltage Control	$k_{\mathrm{P,V}}$	0.09
I. Time Constant - Current Control	$T_{\mathrm{i,I}}$	0.02 s
I. Time Constant - Voltage Control	$T_{\mathrm{i,V}}$	0.005 s

Mertens, 2019). In case of the vsgPLL control, destabilising effects of the PLL are well illustrated by the additional resonances near the fundamental frequency. In fact, PLL-driven grid-forming approaches can be found in a number of publications, however, these concepts and similar approaches are less common and not recommended due to the additional coupling of the inner voltage control with the VSG control via the PLL-driven feedback path, as elaborated in this paper. An example of this coupling is presented in the next section.

4.2 Application Example

A VSG- and a vsgPLL-controlled converter defined by the parameters in Table 1 are connected via transmission lines with an equivalent impedance of $Z_{\text{line}} = 0.25 + j1.25\,\Omega$ to equally share a load of $P \approx 32\,\text{kW}$. The sequence impedance-based stability analysis of the VSG- and the vsgPLL-controlled converter is illustrated in Fig. 2b in terms of phase (PM) and gain margin (GM) for a PLL bandwidth of $\omega_{\text{BW}} \approx 85\,\text{Hz}$. The distance of the minor feedback $Y_{\text{G}}(s)Z_{\text{VSG/vsgPLL}}(s)$ to the critical point (Nyquist criterion) is marked with a red line which indicates an instability at $f \approx 38\,\text{Hz}$ in contrast to a VSG-only setup (dashed line). This exemplarily illustrated critical mode of a grid-forming converter cluster introduces non-typical grid oscillations with respect to conventional power systems based on large synchronous generators.

In Fig. 3, this analysis is verified by time-domain simulation starting with a steady-state operation, where both converter systems share the load based on the classical VSG control. At $t = 4.5\,\text{s}$, one converter is switched to vsgPLL control mode which results in increasing power oscillations for both converters with $f \approx 12\,\text{Hz}$. These oscillations occur due to the unstable operation point of $\boldsymbol{dV}(s)$ at $f \approx 38\,\text{Hz}$ in combination with the fundamental current at $f = 50\,\text{Hz}$. The stability region as well as the frequency, at which an instability occurs, can be analysed by the derived models in an impedance-based modelling framework.

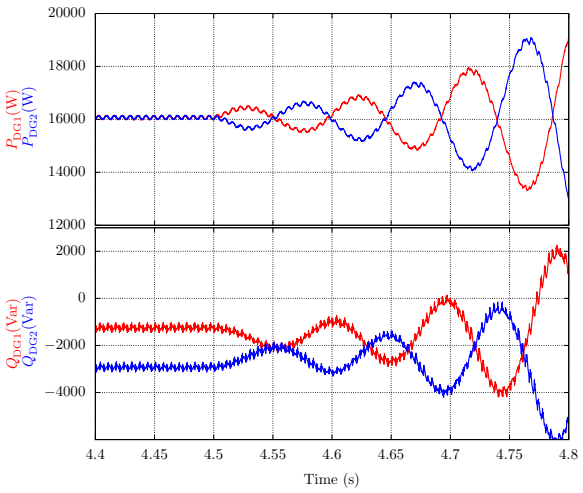

Fig. 3. Transient simulation: Power oscillations of a VSG and vsgPLL-controlled converter sharing a load

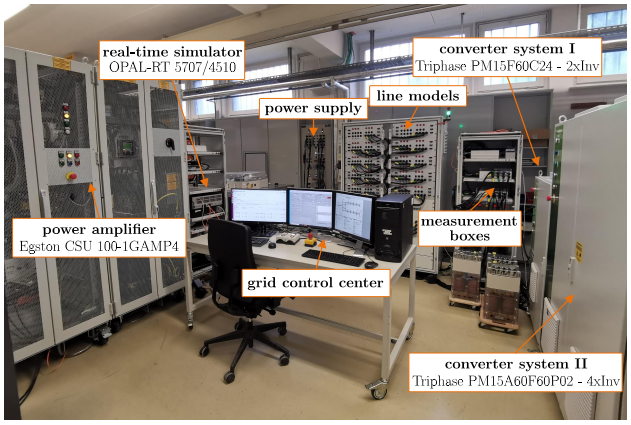

Fig. 4. IAL Microgrid: Picture of the laboratory setup

5. EXPERIMENTAL RESULTS

5.1 Laboratory Setup

In order to further validate the derived models, laboratory experiments have been performed at the IAL Microgrid test bench. The basic experimental setup is shown in Fig. 4, which can be utilised to analyse a variety of different converter-dominated power system aspects. Two Triphase converter systems PM15, each consisting of up to 4 programmable industrial inverters, each with a rated power of 16 kVA and a switching frequency of 16 kHz, can be equipped with LC or LCL filter in order to verify different grid-feeding and grid-following control methods. A four-quadrant digital power amplifier CSU 100 manufactured by Egston (rated power 100 kVA, switching frequency 125 kHz) can be used along with two OPAL-RT real-time simulators OP5707/OP4510 with the objective to establish a P-HIL setup. A rack with 10 modular and freely linkable line models (π-equivalents) is the central element of all hardware grid configurations at this test bench. Portable measurement boxes (designed for 3ph nodes) can be in-

Table 2. Experimental Setup Parameters

PARAMETER	SYMBOL	VALUE
Rated Power	P_{N}	16 kW
Rated Voltage	V_{N}	400 V
Rated Frequency	f_{N}	50 Hz
Active Power Reference	P_{ref}	16 kW
Reactive Power Reference	Q_{ref}	5 kVar
Voltage @ steady state	$V_{0,\text{RMS,LL}}$	410.8 V
Power @ steady state	PQ_0	4.3 kW 12.07 kVar
Nominal Frequency	ω_{N}	314.16 $\frac{\text{rad}}{\text{s}}$
Sampling Time	T_{s}	62.5 μs
Filter Inductor	L	1000 μH
Filter Capacitor	C	10 μF
Frequency Droop Coefficient	D_{p}	16.21
Voltage Droop Coefficient	D_{q}	979.80
Virtual Frequency Inertia	J_{p}	0.129
Virtual Voltage Inertia	J_{q}	7.797
Nominal Frequency of DSOGI Filter	$\omega_{\text{N,DSOGI}}$	314.16 $\frac{\text{rad}}{\text{s}}$
P. Gain - DSOGI Filter	k	$\sqrt{2}$
P. Gain - PLL	$k_{\text{P,PLL}}$	533.3
I. Time Constant - PLL	$T_{\text{i,PLL}}$	–
P. Gain - Current Control	$k_{\text{P,I}}$	0.4234
P. Gain - Voltage Control	$k_{\text{P,V}}$	0.1417
I. Time Constant - Current Control	$T_{\text{i,I}}$	–
I. Time Constant - Voltage Control	$T_{\text{i,V}}$	0.0005 s

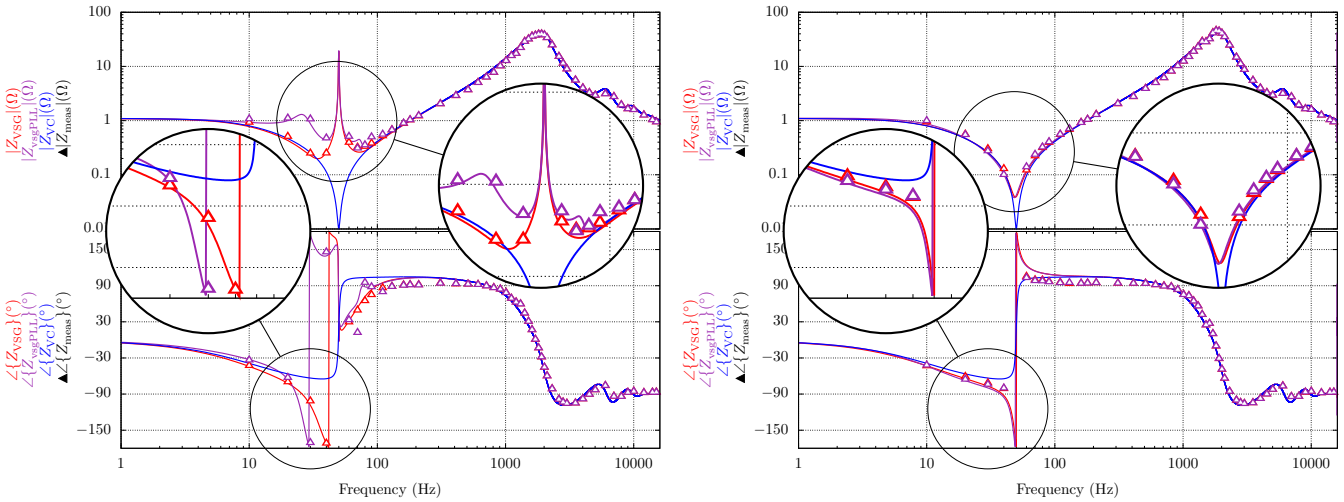

(a) Frequency sweep from 1 Hz to 16 kHz for positive-sequence impedance of voltage-controlled converter $Z_{\mathrm{VC}}(s)$, VSG-controlled converter $Z_{\mathrm{VSG}}(s)$, vsgPLL-controlled converter $Z_{\mathrm{vsgPLL}}(s)$ and experimental results $Z_{\mathrm{meas}}(s)$

(b) Frequency sweep from 1 Hz to 16 kHz for negative-sequence impedance of voltage-controlled converter $Z_{\mathrm{VC}}(s)$, VSG-controlled converter $Z_{\mathrm{VSG}}(s)$, vsgPLL-controlled converter $Z_{\mathrm{vsgPLL}}(s)$ and experimental results $Z_{\mathrm{meas}}(s)$

Fig. 5. Experimental validation of sequence impedance characteristics of grid-forming converters based on VSG and vsgPLL control methods, whose parameters are listed in Table 2

stalled at different nodes within the considered network, while a synchronised measurement can be triggered using National Instruments DAQmx devices.

Both considered control methods (VSG and vsgPLL) are implemented on one converter of the second Triphase converter system (rated current 24 A, rated voltage 400 V) utilising an LC filter. The inner control loop is implemented as a dual voltage loop with active damping but without any harmonic control, while the most relevant parameters are listed in Table 2. In contrast to the previously considered converter, the applied control system introduces a delay of three time steps instead of one. The power amplifier is directly connected to this converter and is operated as an ideal current source, whose reference value is dictated by the real-time simulator. This combination provides the possibility to synchronise the current-controlled power amplifier with the existing converter output voltage in order to (a) achieve a specific steady-state operation point (PQ at the converter terminal) and (b) introduce a small-signal current disturbance to extract the converter output characteristics. The measurements are performed using three Testec TT SI9110 voltage probes (100 MHz/1000 Vrms AC/2% accuracy) and three Keysight N2783B current probes (100 MHz/30 Arms AC/1% accuracy) linked to an LeCroy HDO8108A oscilloscope (sampled with 1 MHz).

5.2 Experimental Results

A frequency sweep is performed to extract the small-signal sequence characteristics of these converters following a specific startup procedure: (1) VSG/vsgPLL: converter starts operating; (2) power amplifier: PLL-based synchronisation employing the real-time simulator; (3) power amplifier: setting of steady-state operation point in PLL mode; (4) power amplifier: transition from PLL to constant current mode with $f = f_{\mathrm{N}}$; (5) power amplifier: injection of positive- or negative-sequence current disturbance and (6) data acquisition. In order to obtain a higher accuracy, five measurements are performed for each frequency, processed and transformed in sequence domain, while step (5) - (6) is repeated for the next measurement set. In general, small standard deviations are obtained with this setup ($\approx 2\%$ of mean value; analogue to measurement accuracy), which is why the average over these frequency sets is further used in the evaluation process and the results are presented without any error bars.

The proposed models are compared with experimental results separately for positive- and negative-sequence impedances as amplitude and phase in Fig. 5. Similar characteristics as for the previous case in Fig. 2a can be identified. In particular, PLL-based feedback (in the power-related control) introduces additional resonances near the fundamental frequency, which are only manifested in positive sequence, since negative sequence is not used to transmit power. Thereby, the negative-sequence impedance is closely related to the inner dual voltage loop control. In addition, the active damping scheme seems to be more effective in positive than negative sequence, whereas additional time delays in the control decrease the total damping performance. Overall, a high model fidelity is achieved with some minor deviations at e.g. $f = 70$ Hz which, however, do not diminish the applicability of these models for large power system stability analysis, especially with respect to the typical uncertainties in these systems.

6. CONCLUSION

In this paper, an equivalent impedance model of two VSG-based control methods has been derived, analysed and verified by time-domain simulations and P-HIL experiments. In particular, the Thévenin equivalent of a voltage-controlled converter is merged with an overlaying VSG control by linearising for a specific operation point. A simulated and experimental frequency sweep and an example analysis verify this modelling approach. In addition,

the analogy between droop and standard VSG control is illustrated as well as the destabilising effects of utilising a PLL as feedback within the outer power control loop. Furthermore, the derived models can be easily coupled with other sequence impedance-based models towards a common simulation framework.

ACKNOWLEDGEMENTS

This work was funded by the Deutsche Forschungsgemeinschaft (DFG, German Research Foundation) project identification number 359921210

REFERENCES

Ahn, S., Park, J., Chung, I., et al. (2010). Power-sharing method of multiple distributed generators considering control modes and configurations of a microgrid. *IEEE Transactions on Power Delivery*, 25(3), 2007–2016.

Amin, M. and Molinas, M. (2017). Small-signal stability assessment of power electronics based power systems: A discussion of impedance- and eigenvalue-based methods. *IEEE Transactions on Industry Applications*, 53(5), 5014–5030. doi:10.1109/TIA.2017.2712692.

Chandorkar, M.C., Divan, D.M., and Adapa, R. (1993). Control of parallel connected inverters in standalone ac supply systems. *IEEE Transactions on Industry Applications*, 29(1), 136–143.

Dokus, M. and Mertens, A. (2019). Sequence impedance-based stability analysis of droop-controlled ac microgrids. In *2019 IEEE 10t PEDG*, 768–773.

Farrokhabadi, M., Canizares, C.A., Simpson-Porco, J.W., et al. (2019). Microgrid stability definitions, analysis, and examples. *IEEE Transactions on Power Systems*.

Harnefors, L., Bongiorno, M., and Lundberg, S. (2007). Input-admittance calculation and shaping for controlled voltage-source converters. *IEEE Transactions on Industrial Electronics*, 54(6), 3323–3334.

Harnefors, L., Finger, R., Wang, X., Bai, H., and Blaabjerg, F. (2017). Vsc input-admittance modeling and analysis above the nyquist frequency for passivity-based stability assessment. *IEEE Transactions on Industrial Electronics*, 64(8), 6362–6370.

Harnefors, L., Wang, X., Yepes, A.G., and Blaabjerg, F. (2016). Passivity-based stability assessment of grid-connected vscs: An overview. *IEEE Journal of Emerging and Selected Topics in Power Electronics*, 4(1), 116–125.

Kabalan, M., Singh, P., and Niebur, D. (2017). Large signal lyapunov-based stability studies in microgrids: A review. *IEEE Transactions on Smart Grid*, 8(5), 2287–2295.

Kundur, P., Paserba, J., Ajjarapu, V., et al. (2004). Definition and classification of power system stability ieee/cigre joint task force on stability terms and definitions. *IEEE Transactions on Power Systems*, 19(3), 1387–1401.

Olivares, D.E., Mehrizi-Sani, A., Etemadi, A.H., et al. (2014). Trends in microgrid control. *IEEE Transactions on Smart Grid*, 5(4), 1905–1919.

Paice, A. and Meyer, M. (2000). Rail network modelling and stability: The input admittance criterion. In *14th Int. Symp. Math. Theory Netw. Syst.*, 1–6.

Pan, D., Wang, X., Liu, F., and Shi, R. (2019). Transient stability of voltage-source converters with grid-forming control: A design-oriented study. *IEEE Journal of Emerging and Selected Topics in Power Electronics*, 1–1. doi:10.1109/JESTPE.2019.2946310.

Parker, S.G., McGrath, B.P., and Holmes, D.G. (2014). Regions of active damping control for lcl filters. *IEEE Transactions on Industry Applications*, 50(1), 424–432.

Rasheduzzaman, M., Mueller, J.A., and Kimball, J.W. (2014). An accurate small-signal model of inverter-dominated islanded microgrids using *dq* reference frame. *IEEE Journal of Emerging and Selected Topics in Power Electronics*, 2(4), 1070–1080.

Rocabert, J., Luna, A., Blaabjerg, F., and Rodriguez, P. (2012). Control of power converters in ac microgrids. *IEEE Transactions on Power Electronics*, 27(11), 4734–4749.

Sarstedt, M., Dokus, M., Gerster, J., et al. (2019). Standardized evaluation of multi-level grid control strategies for future converter-dominated electric energy systems. *at-Automatisierungstechnik*, 67(11), 936–957. doi:10.1515/auto-2019-0061.

Shakerighadi, B., Ebrahimzadeh, E., Blaabjerg, F., and Bak, C.L. (2018). Lyapunov- and eigenvalue-based stability assessment of the grid-connected voltage source converter. In *2018 IEEE International Power Electronics and Application Conference and Exposition (PEAC)*.

Teodorescu, R., Liserre, M., and Rodriguez, P. (2010). *Grid Converters for Photovoltaic and Wind Power Systems*. John Wiley and Sons, Ltd.

Vasquez, J.C., Guerrero, J.M., Savaghebi, M., Eloy-Garcia, J., and Teodorescu, R. (2013). Modeling, analysis, and design of stationary-reference-frame droop-controlled parallel three-phase voltage source inverters. *IEEE Transactions on Industrial Electronics*, 60(4), 1271–1280.

Vieto, I. and Sun, J. (2018). Sequence impedance modeling and converter-grid resonance analysis considering dc bus dynamics and mirrored harmonics. In *2018 IEEE 19th COMPEL*, 1–8.

Wang, S., Liu, Z., and Liu, J. (2018). Modeling of d-q small-signal impedance of virtual synchronous generator. In *2018 IEEE PEAC*, 1–6.

Wang, X., Blaabjerg, F., and Loh, P.C. (2015). Virtual rc damping of lcl-filtered voltage source converters with extended selective harmonic compensation. *IEEE Transactions on Power Electronics*, 30(9), 4726–4737.

Wang, X., Blaabjerg, F., and Loh, P.C. (2017). Passivity-based stability analysis and damping injection for multiparalleled vscs with lcl filters. *IEEE Transactions on Power Electronics*, 32(11), 8922–8935.

Wang, X., Blaabjerg, F., and Wu, W. (2014). Modeling and analysis of harmonic stability in an ac power-electronics-based power system. *IEEE Transactions on Power Electronics*, 29(12), 6421–6432.

Wang, X., Harnefors, L., and Blaabjerg, F. (2018). Unified impedance model of grid-connected voltage-source converters. *IEEE Transactions on Power Electronics*, 33(2), 1775–1787.

Wu, H., Ruan, X., Yang, D., et al. (2016). Small-signal modeling and parameters design for virtual synchronous generators. *IEEE Transactions on Industrial Electronics*, 63(7), 4292–4303.